[^{13}C,^{13}C]- and [^{13}C,^{1}H]-TROSY in a Triple Resonance Experiment for Ribose−Base and Intrabase Correlations in Nucleic Acids[1]

Roland Riek,[†] Konstantin Pervushin,[†] César Fernández,[†] Masatsune Kainosho,*[,‡] and Kurt Wüthrich*[,†]

Contribution from the Institute für Molekularbiologie and Biophysik, Eidgenössische Technische Hochschule Hönggerberg, CH-8093 Zürich, Switzerland, and Department of Chemistry, Faculty of Science, Tokyo Metropolitan University, 1-1 Minamiohsawa, Hachioji, Tokyo 192-03, Japan

Received October 27, 1999. Revised Manuscript Received October 11, 2000

Abstract: A novel TROSY (transverse relaxation−optimized spectroscopy) element is introduced that exploits cross-correlation effects between ^{13}C−^{13}C dipole−dipole (DD) coupling and ^{13}C chemical shift anisotropy (CSA) of aromatic ring carbons. Although these ^{13}C−^{13}C effects are smaller than the previously described [^{13}C,^{1}H]-TROSY effects for aromatic ^{13}C−^{1}H moieties, their constructive use resulted in further transverse relaxation−optimization by up to 15% for the resonances in a 17 kDa protein−DNA complex. As a practical application, two- and three-dimensional versions of the HCN triple resonance experiment for obtaining ribose−base and intrabase correlations in the nucleotides of DNA and RNA (Sklenar, V.; Peterson, R. D.; Rejante, M. R.; Feigon, J. *J. Biomol. NMR* **1993**, *3*, 721−727) have been implemented with [^{13}C,^{1}H]- and [^{13}C,^{13}C]-TROSY elements to reduce the rate of transverse relaxation during the polarization transfers between ribose ^{13}C1′ and base ^{15}N1/9 spins, and between ^{13}C6/8 and N1/9 within the bases. The resulting TROSY-HCN experiment is user-friendly, with a straightforward, robust experimental setup. Compared to the best previous implementations of the HCN experiment, 2-fold and 5-fold sensitivity enhancements have been achieved for ribose−base and intrabase connectivities, respectively, for ^{13}C,^{15}N-labeled nucleotides in structures with molecular weights of 10 and 17 kDa. TROSY-HCN experiments should be applicable also with significantly larger molecular weights. By using modified TROSY-HCN schemes, the origins of the sensitivity gains have been analyzed.

Introduction

Resonance assignment of DNA and RNA by intranucleotide and sequential nuclear Overhauser effects[2] has in recent years been supplemented and in part replaced by the use of heteronuclear correlation experiments for obtaining ribose−base correlations,[3−9] sequential backbone assignments[10−15] and ^{1}H−^{1}H correlations within the bases,[16−20] and the detection of scalar couplings across hydrogen bonds.[21,22] Compared to the corresponding work with proteins, the introduction of heteronuclear NMR experiments with nucleic acids has been delayed by the slower development of techniques for the preparation of ^{13}C- and ^{15}N-labeled oligonucleotides.[23−26] In oligonucleotides, ^{13}C−^{15}N scalar coupling constants are small (up to 12 Hz), so that

* Address correspondence to this author.
† Eidgenössische Technische Hochschule.
‡ Tokyo Metropolitan University.

(1) Abbreviations: CRINEPT, cross-correlated relaxation-enhanced polarization transfer; CSA, chemical shift anisotropy; INEPT, insensitive nuclei enhanced by polarization tranfer; DD, dipole−dipole; TROSY transverse relaxation−optimized spectroscopy; [^{13}C,^{1}H]-TROSY, TROSY using cross-correlation between ^{13}C CSA and ^{13}C−^{1}H DD coupling; [^{13}C,^{13}C]-TROSY, TROSY using cross-correlation between ^{13}C CSA and ^{13}C-^{13}C DD coupling; 2D and 3D, two and three dimensional.

(2) Wüthrich, K. *NMR of Proteins and Nucleic Acids;* Wiley: New York, 1986.
(3) Sklenar, V.; Peterson, R. D.; Rejante, M. R.; Feigon, J. *J. Biomol. NMR* **1993**, *3*, 721−727.
(4) Farmer, B. T.; Müller, L.; Nikonowicz, E. P.; Pardi, A. *J. Am. Chem. Soc.* **1993**, *115*, 11040−11041.
(5) Sklenar, V.; Peterson, R. D.; Rejante, M. R.; Feigon, J. *J. Am. Chem. Soc.* **1993**, *115*, 12181−12182.
(6) Farmer, B. T.; Müller, L.; Nikonowicz, E. P.; Pardi, A. *J. Biomol. NMR* **1994**, *4*, 129−133.
(7) Sklenar, V.; Dieckmann, T.; Butcher, S. E.; Feigon, J. *J. Magn. Reson.* **1998**, *130*, 119−124.
(8) Tate, S.; Ono, A.; Kainosho, M. *J. Am. Chem. Soc.* **1994**, *116*, 5977−5978.
(9) Fiala, R.; Jiang, F.; Sklenar, V. *J. Biomol. NMR* **1998**, *12*, 373−383.
(10) Heuss, H. A.; Wijmenga, S. S.; Vandeven, F. J. M.; Hilbers, C. W. *J. Am. Chem. Soc.* **1994**, *116*, 4983−4984.
(11) Marino, J. P.; Diener, J. L.; Moore, P. B.; Griesinger, C. *J. Am. Chem. Soc.* **1997**, *119*, 7361−7366.
(12) Wijmenga, S. S.; Heus, H. A.; Leeuw, H. A. E.; Hope, H.; van der Graaf, M.; Hilbers, C. W. *J. Biomol. NMR* **1995**, *5*, 82−86.
(13) Tate, S.; Ono, A.; Kainosho, M. *J. Magn. Reson.* **1995**, *B106*, 89−91.
(14) Varani, G.; Aboul-ela, F.; Alain, F.; Gubster, C. C. *J. Biomol. NMR* **1995**, *5*, 82−86.
(15) Ramachandran, R.; Sich, C.; Grüne, M; Soskic, V.; Brown, L. R. *J. Biomol. NMR* **1996**, *7*, 251−255.
(16) Simorre, J.-P.; Zimmermann, G. R.; Pardi, A.; Farmer, B. T., II; Müller, L. *J. Biomol. NMR* **1995**, *6*, 427−432.
(17) Fiala, R.; Jiang, F.; Patel, D. J. *J. Am. Chem. Soc.* **1996**, *118*, 689−690.
(18) Sklenar, V.; Dieckmann, T.; Butcher, S. E.; Feigon, J. *J. Biomol. NMR* **1996**, *7*, 83−87.
(19) Simorre, J.-P.; Zimmermann, G. R.; Pardi, A.; Farmer, B. T., II; Mueller, L. *J. Biomol. NMR* **1996**, *6*, 427−432.
(20) Simorre, J.-P.; Zimmermann, G. R.; Mueller, L.; Pardi, A. *J. Am. Chem. Soc.* **1996**, *118*, 5316−53177.
(21) Dingley, A. J.; Grzesiek, S. *J. Am. Chem. Soc.* **1998**, *120*, 8293−8297.
(22) Pervushin, K.; Ono, A.; Fernández, C.; Syzperski, T.; Kainosho, T.; Wüthrich, K. *Proc. Natl. Acad. Sci. U.S.A.* **1998**, *95*, 14147−14151.
(23) Nikonowicz, E. P.; Sirr, A.; Legault, P.; Jucker, F. M.; Baer, L. M.; Pardi, A. *Nucleic Acids Res.* **1992**, *20*, 4507−4513.
(24) Batey, R. T.; Inada, M.; Kujawinski, E.; Puglisi, J. D.; Williamson, J. R. *Nucleic Acids Res.* **1992**, *20*, 4515−4523.
(25) Michnicka, M. J.; Harper, J. W.; King, G. C. *Biochemistry* **1993**, *32*, 395−400.

10.1021/ja9938276 CCC: $20.00
Published on Web 01/03/2001

long polarization transfer periods are required to transfer magnetization between these nuclei, with concomitant loss of signal intensity due to transverse relaxation. Thus, experiments with larger oligonucleotides or oligonucleotide−protein complexes often produce disappointing results, although significantly improved sensitivity has been achieved with the use of multiple-quantum coherences.[7,9,11]

The dominant relaxation mechanisms during polarization transfers between ^{13}C and ^{15}N are dipole−dipole (DD) coupling between ^{1}H and ^{13}C and the chemical shift anisotropy (CSA) of ^{13}C. This paper introduces transverse relaxation−optimized spectroscopy[27] (TROSY) into the HCN triple resonance experiment, which was previously developed for assignments of nucleic acids.[3−9] TROSY reduces transverse relaxation in $^{13}C-^{1}H$ moieties of aromatic rings[28,29] and thus increases the range of potential applications of triple resonance experiments for resonance assignments of uniformly isotope-labeled nucleotides in DNA and RNA to large molecular sizes, as encountered in nucleic acid complexes with proteins and other compounds.

Transverse relaxation−optimization for aromatic $^{13}C-^{1}H$ groups by cross-correlation between $^{1}H-^{13}C$ DD coupling and ^{13}C CSA is less complete than for $^{15}N-^{1}H$ moieties both because the ^{13}C CSA tensors deviate more pronouncedly from axial symmetry than the ^{15}N CSA tensors in amide groups[27] and because aromatic ^{1}H spins have much smaller CSA than amide protons.[28,29] It is therefore of practical interest that this paper introduces a novel TROSY effect that is based on cross-correlation between $^{13}C-^{13}C$ DD coupling and ^{13}C CSA. The combined TROSY effects from cross correlation between $^{13}C-^{13}C$ DD coupling and ^{13}C CSA and from $^{1}H-^{13}C$ DD coupling and ^{13}C CSA result in improved transverse relaxation−optimization, and there is the promise that assignments of ribose−base correlations with TROSY-HCN experiments may be achieved for molecular sizes up to approximately 30 to 50 kDa.

Experimental Section

All NMR experiments in this paper were recorded with the 14-base pair DNA duplex of Figure 1a. The fully and partially $^{13}C,^{15}N$-labeled DNA oligomers were synthesized on a DNA synthesizer (Applied Biosystems model 392-28) by the solid-phase phosphoramidite method using isotope-labeled monomer units that had been synthesized according to a previously described strategy.[26] Approximately 1 μmol of oligomer was obtained from 5 μmol of nucleoside bound to the resin. A NMR sample of the partially labeled DNA duplex at a concentration of about 2 mM was prepared in 90% H_2O/10% D_2O containing 50 mM potassium phosphate and 20 mM KCl at pH 6.0. A NMR sample of the *Antp* homeodomain−DNA complex comprising the fully $^{13}C,^{15}N$-labeled DNA was prepared in the same solvent at a concentration of 0.8 mM. The NMR experiments were recorded on a Bruker DRX 600 spectrometer using a triple resonance probe head equipped with a z-gradient coil. NMR measurements with the free DNA were performed at 20 °C, and those with the *Antp* homeodomain−DNA complex at 15 °C. The instrument settings used are detailed in the figure captions.

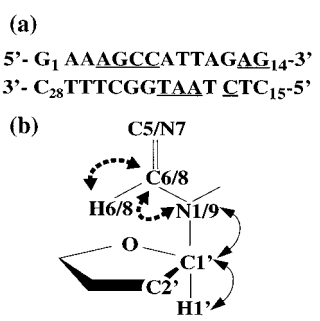

Figure 1. (a) Structure of the DNA duplex used in this study. The duplex was available in the uniformly $^{13}C,^{15}N$-labeled form, which was studied in a complex with the *Antennapedia* homeodomain, and with uniform $^{13}C,^{15}N$-labeling of only the underlined nucleotides, which was studied in the free from. (b) Scheme showing the two magnetization transfer pathways that are simultaneously initiated by the TROSY-HCN experiment of Figure 2. In the double notations, N1, C6, H6, and C5 apply to the pyrimidine bases, and N9, C8, H8, and N7 to the purine bases. Dotted arrows indicate the intrabase transfers and solid arrows the ribose−base transfers.

Methods

Similar to the conventional HCN experiment[3] the TROSY-HCN pulse sequence is based on the two simultaneous coherence flows H1′ → C1′ → N1/9 → C1′ → H1′ and H6/8 → C6/8 → N1/9 → C6/8 → H6/8 (Figure 1b) and provides ribose−base correlations via the $^{15}N1/9$ resonances in a single experiment. Figure 2 shows a scheme for 3D TROSY-HCN, but here we first provide a description of a 2D [$^{15}N,^{1}H$]-version. The experiment starts with polarization on the protons H1′ and H6/8 (Figure 1b), which is transferred to the directly attached carbons via an INEPT step[30] and merged with the ^{13}C steady-state magnetization. The magnetization at time point *a* in Figure 2 is then given by

$$\sigma(a) = uC_x + vC_xH_{z'} \quad (1)$$

where u represents the steady-state magnetization of ^{13}C and v the ^{1}H steady-state magnetization.[28] After the delay Δ the^{13}C magnetization is in antiphase with respect to $^{15}N1/9$. The following 90° pulse on ^{15}N generates heteronuclear double-quantum and zero-quantum coherences. During the time period t_2, ^{15}N is frequency labeled and the REBURP soft pulse[31] on ^{13}C refocuses the precession of C1′ and C6/8. Simultaneously, the REBURP pulse decouples C1′ and C6/8 from other nuclei ($J_{C1'C2'} \approx 45$ Hz, $J_{C6C5} \approx 66$ Hz, $J_{C8C5/4} \approx 8-11$ Hz, $J_{C6C2} \approx 2-3$ Hz, $J_{C1'H1'} \approx 160$ Hz, $J_{C6/8H6/8} \approx 180-225$ Hz).[32] After the second 90°(^{15}N) pulse the magnetization is again in $^{13}C,^{15}N$-antiphase, and is further refocused during the second delay Δ to (point *b* in Figure 2)

$$\sigma(b) = \{(uC_xH_z \sinh[R_C(2\Delta + t_2)]) + vC_xH_z(\cosh[R_C(2\Delta + t_2)])\} \cos[\omega_N t_2] \quad (2)$$

where R_C is the cross-correlated relaxation between ^{13}C CSA and $^{13}C-^{1}H$ DD coupling. As shown in the first term of (2), ^{13}C steady-state magnetization is transferred to $^{1}H-^{13}C$ antiphase magnetization by

(26) Ono, A.; Tate, S.; Kainosho, M. In *Stable Isotope Applications in Biomolecular Structure and Mechanisms*; Trewhella, J. L., Cross, T. A., Unkefer, C. J., Eds.; Los Alamos National Laboratory: Los Alamos, NM, 1994; pp 127−144.
(27) Pervushin, K.; Riek, R.; Wider, G.; Wüthrich, K. *Proc. Natl. Acad. Sci. U.S.A.* **1997**, *94*, 12366−12371.
(28) Pervushin, K.; Riek, R.; Wider, G.; Wüthrich, K. *J. Am. Chem. Soc.* **1998**, *120*, 6394−6400.
(29) Brutscher, B.; Boisbouvier, J.; Pardi, A.; Marion, D.; Simorre, J. P. *J. Am. Chem. Soc.* **1998**, *120*, 11845−11851.
(30) Morris, G. A.; Freeman, R. *J. Am. Chem. Soc.* **1979**, *101*, 760−762.
(31) Geen, H.; Freeman, R. *J. Magn. Reson.* **1991**, *93*, 93−141.
(32) The TROSY-HCN experiment was also performed with two soft pulses on ^{15}N, at the positions of the vertical dotted lines in Figure 2, to decouple the small spin−spin couplings $^{13}C8-^{15}N7$ ($J_{C8N7} < 3$ Hz: Ippel, J. H.; Wijmenga, S. S.; de Jong, R.; Heus, H. A.; Hilbers, C. W.; de Vroom, E.; van der Marel, G. A.; van Boom, J. H. *Magn. Reson. Chem.* **1996**, *34*, 156−176. Kainosho, M., et al., unpublished results). No measurable difference to the experiment without ^{15}N decoupling was observed (data not shown).

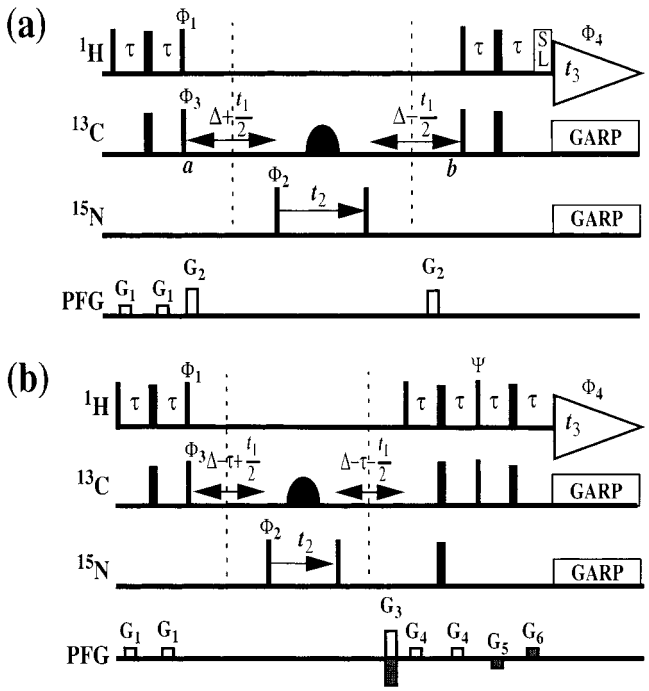

Figure 2. Two 3D TROSY-HCN pulse sequences for use with large molecules (a) or with smaller molecules (b), respectively. For both experimental schemes the parameters are given for a setup at a ^{1}H frequency of 600 MHz. In the rows marked ^{1}H,^{13}C, and ^{15}N the narrow and wide bars stand for nonselective 90° and 180° radio frequency pulses, respectively. The black curved shape is a REBURP-2 pulse[31] on ^{13}C of duration 3.3 ms, with additional cosine modulation (f_m = 4000 Hz) to provide simultaneous inversion at 85 ± 4.3 and 140 ± 4.3 ppm. GARP decoupling[47] on ^{13}C and ^{15}N was used during acquisition. The ^{1}H, ^{13}C, and ^{15}N carrier frequencies are at 4.7 ppm (on-resonance to water) and 113 and 158 ppm, respectively. The delay τ = 1.25 ms is a compromise between $^1/_4J_{C1'H1'}$ and $^1/_4J_{C6/8\,H6/8}$ ($J_{C1'H1'} \approx 160$ Hz, $J_{C6/8\ H6/8}$ = 180−225 Hz**)**, and the delay Δ = 25 ms is adjusted for optimal sensitivity. Pulse phases: $\Phi_1 = y$; $\Phi_2 = x, -x$; $\Phi_3 = x$; $\Phi_4 = x, -x$, and x otherwise. In part a, a spin-lock pulse of length 0.75 ms was used to suppress the water resonance,[48] and Φ_2 and Φ_3 are incremented in a States-TPPI manner to achieve quadrature detection in the ^{15}N and ^{13}C frequency dimensions.[49] In part b, combination of a change in the sign of the pulsed field gradient G_3 with $\Psi = y$ or $-y$ yields a pure-phase absorption spectrum.[50] In a 2D version of experiment (a) we set t_1 to zero and the States-TPPI was applied only to Φ_2. The rows marked PFG (pulsed field gradient) indicate the magnetic field gradients applied along the z-axis: G_1, amplitude = 3 G/cm, duration = 0.4 ms; G_2, amplitude = 6 G/cm, duration = 0.3 ms; G_3, amplitude = −15 G/cm, duration = 1.75 ms; G_4, amplitude = 15 G/cm, duration = 0.4 ms; G_5, amplitude = −15 G/cm, duration = 0.22 ms; $G_6 = -G_5$; note that $G_5 + G_6 = \gamma_C/\gamma_H G_3$. The two vertical dotted lines indicate the center of the time periods Δ and are used as a reference for discussions in the text. We would like to add that the radio-frequency pulses and the delays on the ^{13}C channel are programmed in parallel with the radio-frequency pulses on ^{15}N, which allows the first increment on ^{15}N to be set to a half-dwell. Otherwise, phase problems along t_2 would occur due to the use of a REBURP-2 pulse[31] of duration 3.3 ms on ^{13}C.

cross-correlated relaxation.[43] Finally, after the ^{1}H−^{15}N INEPT step the ^{1}H1′/H6/H8 signals are acquired during the period t_3. Since no ^{1}H pulses are applied between *a* and *b*, [^{13}C,^{1}H]-TROSY is active during the entire period $2\Delta + t_2$.[27,28]

In the 3D version of the TROSY-HCN experiment (Figure 2) the ^{13}C1′ and ^{13}C6/8 nuclei are frequency labeled in a semiconstant time manner during the time period t_1. The ^{1}H steady-state magnetization and the ^{13}C steady-state magnetization are both used, which provides enhanced sensitivity and further supports the suppression of the rapidly relaxing component of the ^{13}C doublet.[28] As a consequence, when compared to the corresponding conventional experiments, the ^{13}C−^{1}H cross-peaks are upfield-shifted by 0.5 $^1J_{CH}$ in the ω_1(^{13}C) dimension. The scalar couplings $^1J_{C1'C2}$, $^1J_{C6C5}$, $^1J_{C6N1}$, and $^1J_{C8N9}$ are not refocused during the evolution period t_1. This does not result in line-broadening as long as the maximal evolution time, $t_{1,max}$, is shorter than about 4 ms. The calculated line-broadening for an evolution time of $t_{1,max}$ = 4 ms is less than 5%. This condition was met in all of our 3D experiments. With evolution times longer than 4 ms, line-broadening due to splitting of the cross-peaks would occur, as was demonstrated by Grzesiek and Bax[33] in the case of $^1J_{C\alpha C\beta}$ in proteins.

Recently, a sensitivity-enhanced TROSY pulse sequence for correlating aromatic carbons with protons was published,[34] which uses a modified ST2-PT element[35] with two INEPT steps to refocus the carbon magnetization and then transfer it back to protons. An average sensitivity gain of 22% was reported to result from this modification for the 10 kDa protein RAP(18-112). A concatenated implementation[36] of the modified ST2-PT element into the TROSY-HCN experiment of Figure 2a (Figure 2b) yielded gains of 0−35% for individual resonance lines in our 10 kDa DNA duplex. For the 18 kDa *Antp* homeodomain−DNA complex the two experiments yielded comparable data, where different individual peaks would be favored by the scheme of either Figure 2a or Figure 2b. Overall, based on our current experience we present two alternatives in Figure 2, since the 3D sensitivity-enhanced TROSY-HCN experiment of Figure 2b yields superior results for structures with molecular weights up to approximately 10 kDa, the 3D versions of the two experiments provide comparable sensitivity for larger molecules, and the 2D version of the scheme of Figure 2a (see Figures 3 and 4) gives superior results in all situations. In the following we further analyze the observed sensitivity difference for the two 2D TROSY-HCN experiments of Figure 2, a and b. On the basis of the product operator formalism[37] for a two-spin system with a strong TROSY effect, with neglect of the anti-TROSY component, both schemes should be equal in sensitivity. However, although the anti-TROSY component is about one order of magnitude less intense than the TROSY component, it is not negligibly small. Since in the scheme of Figure 2a the anti-TROSY component is added, and in the scheme of Figure 2b it is suppressed, the pulse sequence of Figure 2a is thus intrinsically more sensitive. In the scheme of Figure 2b further sensitivity may be lost due to non-perfect gradient-refocusing, additional transverse relaxation, and additional passive couplings (see above) that are active during the additional INEPT step. Finally, during the additional INEPT step with the delay 2τ, the antiphase coherences are not completely refocused, since the range of scalar couplings is quite large ($J_{C1'H1'} \approx 160$ Hz, $J_{C6/8H6/8}$ = 180−225 Hz) and concomitantly the choice of the delay τ is only a compromise for acceptable performance over the entire range of J-values.

Results

TROSY-HCN (Figure 2) measurements have been compared with corresponding data obtained with the original HCN experiments[3] and with a previously described improved scheme that makes use of multiple quantum coherences (MQ-HCN).[9]

(33) Grzesiek, S.; Bax, A. *J. Magn. Reson.* **1992**, *96*, 432−440.
(34) Meissner, A.; Sørensen, O. W. *J. Magn. Reson.* **1999**, *139*, 439−442. Meissner, A.; Sørensen, O. W. *J. Magn. Reson.* **2000**, *144*, 171−174.
(35) Pervushin, K. V.; Wider, G.; Wüthrich, K. *J. Biomol. NMR* **1998**, *12*, 345−348.
(36) Salzmann, M.; Wider, G.; Pervushin, K.; Wüthrich, K. *J. Biol. NMR* **1999**, *15*, 182−185.
(37) Sørensen, O. W.; Eich, G. W.; Levitt, M. H.; Bodenhausen, G.; Ernst, R. R. *Prog. NMR Spectrosc.* **1983**, *16*, 163−192.
(38) Fernández, C.; Szyperski, T.; Ono, A.; Iwai, H.; Tate, S.; Kainosho, M.; Wüthrich, K. *J. Biomol. NMR* **1998**, *12*, 25−37.
(39) Wüthrich, K. *Nature Struct. Biol.* **1998**, *5*, 492−495.
(40) Fiala, R.; Czernek, J.; Sklenar, V. *J. Biomol. NMR* **2000**, *16*, 291−302.
(41) Salzmann, M.; Pervushin, K.; Wider, G.; Wüthrich, K. *Proc. Natl. Acad. Sci. U.S.A.* **1998**, *95*, 13585−13590.
(42) Salzmann, M.; Pervushin, K.; Wider, G.; Wüthrich, K. *J. Am. Chem. Soc.* **2000**, *122*, 7443−7548.
(43) Riek, R.; Wider, G.; Pervushin, K.; Wüthrich, K. *Proc. Natl. Acad. Sci. U.S.A.* **1999**, *96*, 4918−4923.

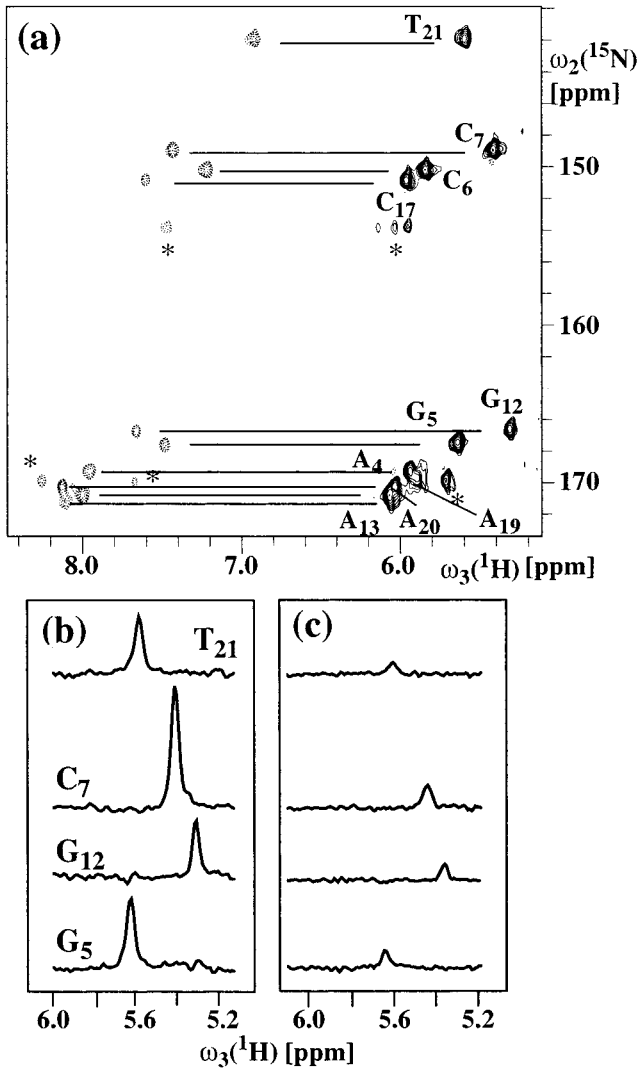

Figure 3. 2D TROSY-HCN spectrum ($t_1 = 0$ in Figure 2) of the partially ^{13}C,^{15}N-labeled DNA duplex of Figure 1a free in solution. (a) Contour plot. Correlations between riboses and bases are indicated by horizontal lines and individually assigned. Some impurities due to slow degradation of the sample are marked by asterisks. (b) Cross-sections along $\omega_3(^1H)$ through the cross-peaks of four nucleotides in the 2D TROSY-HCN spectrum. (c) Corresponding cross-sections to those in part b from a spectrum recorded with the original HCN experiment.[3] The measuring time for both experiments was 0.5 h; the acquired data size was 75 × 512 complex points, with t_{2max}= 24 ms and t_{3max}= 85 ms. For the conventional HCN experiment[3] the delays $\Delta = 25$ ms and $\tau = 1.6$ ms (optimized value for $^1/_4J_{C1'H1'}$) were used, and the ^{13}C carrier frequency was at 85 ppm. Negative intensities are displayed with broken contour lines and positive intensities with solid contour lines, respectively.

Ribose−base correlations via the $^{15}N1/9$ resonances for the purine and pyrimidine nucleotides were studied in both the DNA duplex of Figure 1a free in solution, which has a molecular weight of 10 kDa, and a complex of this duplex with the *Antp* homeodomain, which has a molecular weight of 17 kDa (Figures 3−5). Figure 3a shows a contour plot of a 2D TROSY-HCN spectrum recorded with the partially ^{13}C,^{15}N-labeled free DNA duplex (Figure 1a), with the ribose-to-base connections indicated by horizontal lines and the individual resonance assignments.[38] In Figure 3b,c, cross-sections through four peaks connecting H1′ with N1/9 are displayed for TROSY-HCN and the original HCN experiment,[3] respectively. The greatly improved sensitivity of the TROSY-HCN experiment is readily apparent in these

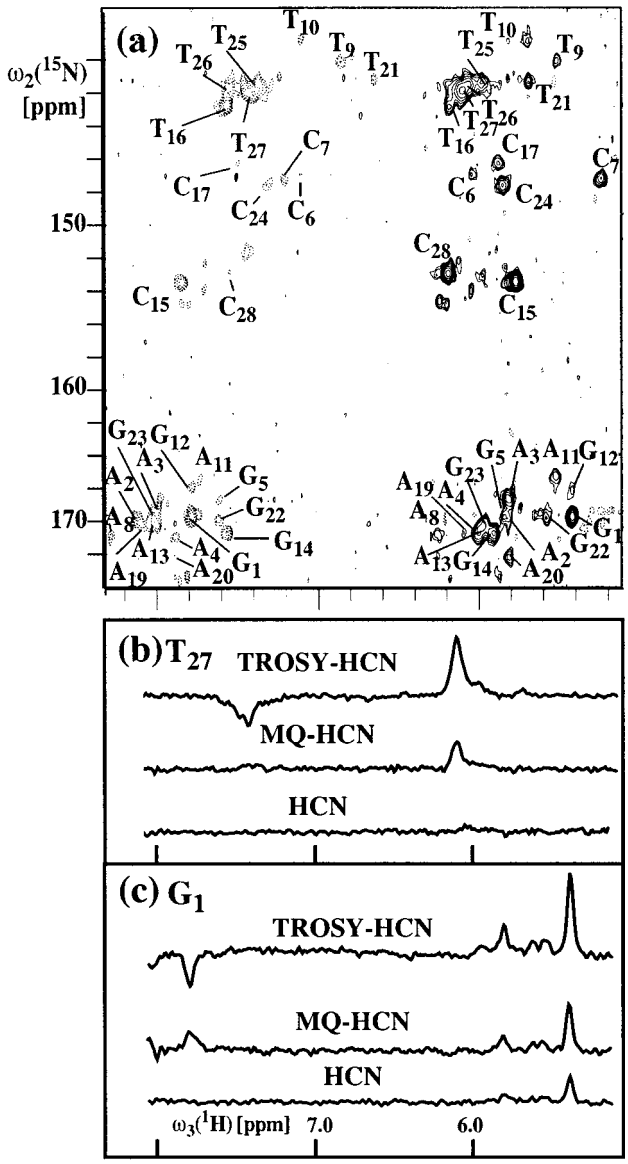

Figure 4. (a) Contour plot of a 2D TROSY-HCN spectrum of the *Antp* homeodomain−DNA complex with the fully ^{13}C,^{15}N-labeled DNA duplex of Figure 1a. The cross-peaks for ribose−base and intrabase correlations are individually assigned, where the intranucleotide connectivities were obtained in part from the 3D TROSY-HCN experiment of Figure 5. The sequence-specific assignments are from Fernández et al.;[38] no assignments are given for T_{18} because its H1′ resonance at 4.68 ppm[38] is under the water resonance. (b and c) Cross sections of T_{27} and G_1 are shown from 2D TROSY-HCN, the 2D MQ-HCN,[9] and the original 2D HCN experiment.[3] The original version of the HCN experiment[3] yields only the H1′−N9/1 correlations. The measuring time for each of the three experiments was 6 h, and the acquired data size was 75 × 512 complex points, with $t_{2max} = 24$ ms and $t_{3max} = 85$ ms. For 2D MQ-HCN two subspectra were collected, one of which was optimized for ribose−base correlations and the other one for intrabase correlations.[9] In part a, negative intensities are displayed with broken contour lines and correspond to intrabase correlations. Positive intensities are displayed with solid contour lines and correspond to ribose−base correlations.

spectra, which were recorded in 0.5 h. A quantitative assessement revealed a 4-fold gain in the signal-to-noise ratio relative to the HCN scheme[3] and a 2-fold gain relative to MQ-HCN[9] (Table 1). The sensitivity improvement is yet more pronounced in the spectra of the *Antp* homeodomain−DNA complex (Figure 4). Whereas in the TROSY-HCN spectrum all expected cross-peaks are detected (Figure 4a), only the resonances of the chain-

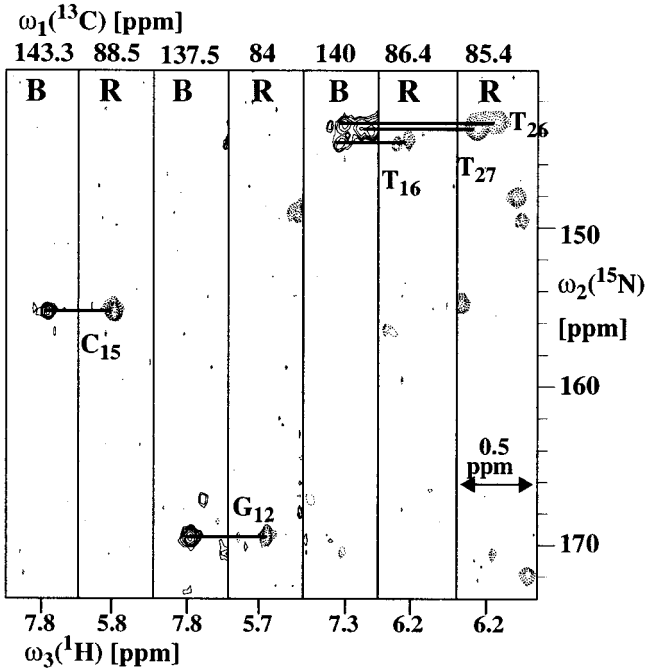

Figure 5. Strips taken from a 3D TROSY-HCN experiment with the *Antp* homeodomain−DNA complex with the fully $^{13}C,^{15}N$-labeled DNA duplex of Figure 1a. The ribose peaks are identified, and the correlations between riboses (R) and bases (B) are indicated by horizontal lines. The measuring time was 15 h and the acquired data size was 43 × 75 × 512 complex points, with t_{1max} = 4.5 ms, t_{2max} = 24 ms, and t_{3max}= 85 ms.

terminal nucleotides were observed with the original HCN scheme,[3] and although a complete set of ribose−base correlation peaks was observed with MQ-HCN[9] the intrabase cross-peaks were weak when compared with TROSY-HCN (Figure 4b,c). A quantitative comparison of TROSY-HCN with MQ-HCN (Table 1) yielded a 2-fold gain in sensitivity for ribose−base correlations, and a 5-fold gain for intrabase correlations.

To illustrate the use of 3D TROSY-HCN, Figure 5 shows strips along $\omega_2(^{15}N)$ of a 3D TROSY-HCN spectrum of the *Antp* homeodomain−DNA complex measured in 15 h, where the correlations between the ribose H1′−C1′ moieties and the base H6/8−C6/8 moieties via the N1/9 chemical shifts are clearly manifested.

Discussion

The data presented in the Figures 3−5 demonstrate that compared to previous implementations, a further gain in sensitivity can be achieved with the use of [$^{13}C,^{1}H$]- and [$^{13}C,^{13}C$]-TROSY in HCN-type triple resonance experiments for resonance assignments in $^{13}C,^{15}N$-labeled DNA- or RNA-nucleotides.[3−6,8,17] For a DNA duplex with molecular weight 10 000 free in solution, a 2-fold gain in sensitivity was thus achieved for the ribose−base correlations, whereby the TROSY experiment yields the ribose−base and partial intrabase connectivities in a single measurement. When the same 10 kDa DNA duplex was studied in a 17 kDa complex with a protein, assignments for all nucleotides were obtained with the 2D TROSY-HCN scheme (Figure 4), whereas numerous correlation peaks could not be identified with the other HCN implementations (Table 1). Figure 5 further illustrates that the use of a 3D version of the TROSY-HCN experiment is a practical alternative in situations of signal overlap in the corresponding 2D HCN spectra (Figures 4 and 5). From comparison of the results obtained with the 10 kDa and 17 kDa test samples and from general considerations on the TROSY technique,[27,39] we anticipate that the TROSY-HCN scheme of Figure 2 will be useful also for assignments of $^{13}C,^{15}N$-labeled nucleotides in significantly larger structures, perhaps up to the range 30−50 kDa.

As mentioned previously, the signal attenuation in HCN experiments due to transverse relaxation by $^{1}H-^{13}C$ DD coupling has been significantly reduced in pulse schemes that generate, instead of single-quantum coherences, $^{1}H-^{13}C$ zero-quantum and double-quantum coherences, where there is no DD coupling.[7,9,11] Compared to the original HCN sequence, 2- to 4-fold improvements of the signal-to-noise ratio were thus achieved (Figure 4, Table 1). Drawbacks of this alternative to the use of TROSY are that two measurements are needed with different selective ^{1}H decoupling to suppress homonuclear and heteronuclear scalar couplings during the multiple-quantum evolution periods,[9] and that ^{13}C steady-state magnetization cannot be used. As a consequence, significant further sensitivity gains can be achieved with TROSY, in particular for the intrabase correlations (Table 1). However, since the TROSY effect for ribose C1′− H1′ is intrinsically less important than that for the ring $^{13}C-^{1}H$ moieties in the bases (Table 1), the use of multiple-quantum coherences may in certain situtations give superior results. This was demonstrated with the out-and-stay experiment HsCNCHHb, which correlates ribose spins with base spins by multiple quantum spin evolution during the polarization transfer from ribose to base and with TROSY during the intrabase polarization transfer on ^{13}C.[40] Relative to the introduction of TROSY elements into 3D triple resonance experiments for assignments of proteins, the sensitivity gains achieved when using the TROSY-HCN scheme of Figure 2 with $^{13}C,^{15}N$-labeled nucleotides compare favorably with the gains achieved here when using 3D TROSY-HNCA with $^{13}C,^{15}N$-labeled proteins.[41] In line with previous use of TROSY for aromatic rings in proteins,[28] significant gains in sensitivity are achieved for molecular weights well below 20 kDa, and assignments of ribose−base correlations will foreseeably be obtainable for molecular sizes up to approximately 30−50 kDa. This limit is well below the molecular weights for which backbone assignments can be achieved with [$^{15}N,^{1}H$]-TROSY elements in triple resonance experiments with $^{2}H,^{13}C,^{15}N$-labeled proteins,[39,42] which is due to the less favorable properties of the $^{13}C-^{1}H$ moieties when compared to amide $^{15}N-^{1}H$ groups. In particular, the deviations of the ^{13}C CSA tensor from axial symmetry are the cause of only partial transverse relaxation−optimization, and the very small CSA for ^{13}C-bound protons makes the use of TROSY during ^{1}H detection unattractive (see the Appendix).[28]

Inspection of the experimental scheme for TROSY-HCN (Figure 2) indicates that in addition to the previously described cross-correlation between $^{1}H-^{13}C$ DD and ^{13}C CSA,[28] the TROSY principle may be operative during the period $2\Delta + t_2$ through previously not considered cross-correlation effects between $^{13}C-^{13}C$ DD and ^{13}C CSA. Both of these two types of cross-correlations reduce transverse relaxation during the polarization transfers and the evolution periods (see also the Appendix). Furthermore, cross-correlated relaxation-enhanced polarization transfer[43] (CRINEPT) is not suppressed during the $^{13}C\rightarrow^{15}N$ and $^{15}N\rightarrow^{13}C$ magnetization transfers. In the following we describe modified TROSY-HCN experimental schemes that were used to estimate the contributions from the different mechanisms to transverse relaxation optimization in TROSY-HCN measurements.

To estimate the sensitivity gain due to [$^{13}C,^{1}H$]-TROSY, an experiment was set up which suppresses [$^{13}C,^{1}H$]-TROSY by

Table 1. Contributions from Different Relaxation Pathways to the Sensitivity Gains Achieved with TROSY-HCN[a]

	free DNA		*Antp* homeodomain−DNA complex	
contribution	R−B[b,c]	intra-B[b,c]	R−B[b,d]	intra-B[b,d]
2D TROSY-HCN[e,f]	1	1	1	1
2D HCN[f]	0.25 (0.15−0.3)		0.1 (0−0.25)[g]	
2D HMQC-HCN[h]	0.5 (0.4−0.6)		0.5 (0.3−0.7)	0.15(0−0.5)[i]
[^{13}C,^{1}H]-TROSY	0.5 (0.4−0.6)	0.2 (0−0.5)[k]	0.4 (0.25−0.5)	0.1 (0−0.5)[i]
[^{13}C,^{13}C]-TROSY[l]	0.8 (0.6−0.9)	0.6 (0.4−0.9)	0.75 (0.6−0.9)	0.3 (0−0.6)[m]
[^{13}C,^{15}N]-CRINEPT	0.9 (0.9−1)	0.9 (0.9−1)	0.9 (0.9−1)	0.9 (0.8−1)

[a] The experiments used to estimate the individual contributions are described in the text. The numbers in the table then indicate the residual relative signal intensities after suppression of the individual contributions listed in the first column. [b] R−B and intra-B indicate ribose−base and intrabase correlations, respectively (see Figure 1b). [c] The signal-to-noise ratios in the 2D TROSY-HCN experiment of Figure 2a varied from 10 to 100 for the individual peaks. [d] The signal-to-noise ratios in the 2D TROSY-HCN experiment varied from 5 to 65 for the individual peaks. [e] For practical reasons (many peaks are not observed by conventional HCN) the 2D TROSY-HCN experiments of Figures 3 and 4 are used as the reference. [f] The ratio of the values given for 2D TROSY-HCN and for 2D HCN[3] represents the relative sensitivity gain obtained with TROSY. [g] For the *Antp* homeodomain−DNA complex only the R−B cross-peaks of the four chain-terminal nucleotides were observed with 2D HCN. [h] The ratio of the values given for 2D TROSY-HCN and for 2D MQ-HCN[9] represents the relative sensitivity gain obtained with TROSY. [i] Only 12 of the 28 expected cross-peaks were observed. [k] Only 13 of the 28 expected cross-peaks were observed. [l] The scheme used introduces passive ^{13}C−^{13}C couplings and therefore the [^{13}C,^{13}C]-TROSY effect is systematically overestimated (see text). [m] Only 21 of the expected 28 cross-peaks were observed.

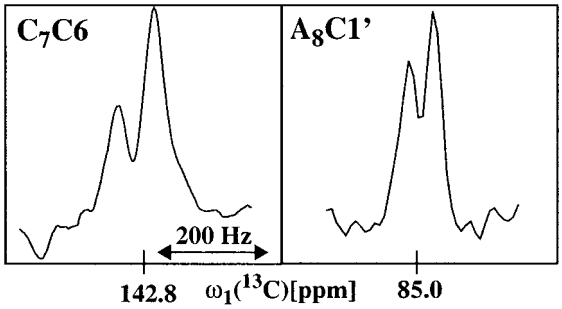

Figure 6. Cross-sections through the base C6−H6 cross-peak of C_7 and the ribose C1′−H1′ cross-peak of A_8 taken along ω_1(^{13}C) from a 2D ct-[^{13}C,^{1}H]-correlation experiment, which was derived from the scheme of Figure 2 by omitting the two 90° pulses on ^{15}N, introducing two IBURP-2 pulses[31] on ^{15}N at the positions indicated by vertical dotted lines, with a duration of 1.65 ms and placed on-resonance at 159 ppm, and by appropriate modification of the phase cycling. To increase the resolution in the ω_1(^{13}C) dimension, the experiment was measured in a semiconstant time manner. The use of the selective 180° REBURP-2 pulse[31] on ^{13}C6/8 and ^{13}C1′ during the constant time period of 25 ms ensured that the ^{13}C−^{13}C couplings as well as [^{13}C,^{13}C]-TROSY were active (see text). The measuring time was 6 h, and the acquired data size was 512 × 1024 complex points, which was zero-filled to 4096 × 2048 points, with t_{1max} = 50 ms and t_{2max} = 85 ms.

application of 180°(^{1}H) pulses in the middle of the delays Δ (dotted vertical lines in Figure 2). On average, a 2-fold reduction of the ribose−base cross-peak intensity and a 5-fold reduction of the intrabase cross-peaks were observed for the free DNA, and the corresponding reductions for the *Antp* homeodomain−DNA complex were 3- and 10-fold, so that only part of the intrabase cross-peaks could be detected (Table 1).

The [^{13}C,^{13}C]-TROSY effect from cross-correlation between ^{13}C−^{13}C DD coupling and ^{13}C CSA was qualitatively evidenced by the different intensities of the multiplet components in a modified [^{13}C,^{1}H]-correlation experiment (see caption to Figure 6), in which [^{13}C,^{13}C]-TROSY is active and the scalar ^{13}C−^{13}C couplings are preserved. The [^{13}C,^{13}C]-TROSY effect is much larger for the pyrimidine ring carbons than for C1′. This observation is in good agreement with model calculations (see the Appendix). Extrapolating from the carbon−carbon multiplet signal ratios in Figure 6 to the 2D TROSY-HCN experiment, where ^{13}C is in the transverse plane for more than 50 ms, we predict a [^{13}C,^{13}C]-TROSY contribution to the measured signal in the *Antp* homeodomain−DNA complex of 25−40% for C6 carbons and <5% for C1′ carbons. Thereby we take into consideration that in TROSY-HCN both doublet components from ^{13}C−^{13}C coupling (Figure 6) contribute to the polarization transfer (in the 2D version this is due to the fact that there is no carbon evolution, and in the 3D version it is due to the limited spectral resolution along ω_1(^{13}C), which prevents detection of the ^{13}C−^{13}C splitting). To access directly the sensitivity improvement due to [^{13}C,^{13}C]-TROSY in the TROSY-HCN experiment, the following pulses were introduced in Figure 2 at the positions indicated with vertical dotted lines: two 180° REBURP-2 pulses on ^{13}C and two 180° IBURP-2 pulses[31] on ^{15}N (centered on-resonance at 159 ppm, with a duration of 1.65 ms). Furthermore, the central 180° REBURP-2 pulse[31] on ^{13}C was replaced by a hard pulse to suppress the cross-correlations between ^{13}C1′ CSA and ^{13}C1′−^{13}C2′ DD coupling, and between ^{13}C6 CSA and ^{13}C6−^{13}C5 DD coupling. A comparison of this 2D "[^{13}C,^{13}C]-TROSY-suppressed" experiment with 2D TROSY-HCN indicates that about 20% of the overall TROSY effect for intrabase correlations and about 5% for ribose−base correlations results from [^{13}C,^{13}C]-TROSY. In drawing this conclusion we allowed for the fact that the pulse scheme used introduces also passive couplings, and therefore, for this experiment, the data given in Table 1 systematically overestimate the [^{13}C,^{13}C]-TROSY contribution. The use of [^{13}C,^{13}C]-TROSY is not limited to the pulse scheme of Figure 2, since this element could readily be incorporated into both the original HCN[3] experiment and the MQ-HCN[9] experiment by applying the same phase for the central ^{13}C hard pulses, 90°(^{13}C)−180°-(^{13}C)− 90°(^{13}C) in these pulse schemes[3,9] and setting the gradients within this pulse trio to the same length. In parts of the original sequences,[3,9] [^{13}C,^{13}C]-TROSY was already active, although this was not explicitly recognized in the respective publications. The general prerequisite of utilizing TROSY effects in other multidimensional experiments is the recognition of potentially interfering relaxation mechanisms of comparable strength. Upon numerical evaluation we found that the ^{13}C−^{13}C dipolar interaction accounts for up to 25% of the CSA interaction, which finds use in many other NMR experiments. The second prerequisite achieve taylored excitation of the magnetization of a given spin in such a way that the other like spin of interest (two carbons in the present case) is not inverted. This results in the preservation of relaxation interference and general sensitivity improvement even when the actual resonance splitting is not observed.

To evaluate a possible role of CRINEPT[43] between ^{13}C and ^{15}N, a 2D TROSY-HCN experiment was measured with suppression of CRINEPT by the addition of two 180° RE-

BURP-2 pulses on ^{13}C and two 180° IBURP-2 pulses on ^{15}N (centered on-resonance at 159 ppm, with a duration of 1.65 ms) at the positions indicated by vertical dotted lines in Figure 2. A comparison with the 2D TROSY-HCN experiment indicated that a possible CRINEPT contribution to the overall sensitivity gain from TROSY in HCN experiments is negligibly small (Table 1).

In conclusion, analysis of the experimental scheme for TROSY-HCN led to the discovery of a novel [^{13}C,^{13}C]-TROSY effect, which has theoretical as well as practical interest. It contributes to make TROSY-HCN an attractive technique for resonance assignments of ^{13}C,^{15}N-labeled DNA and RNA nucleotides. As shown in Table 1, the major sensitivity gains relative to previous implementations of the HCN experiment come from the use of ^{13}C steady-state magnetization and from cross-correlation between $^{13}C-^{1}H$ DD coupling and ^{13}C CSA, but the novel [^{13}C,^{13}C]-TROSY effect makes a significant contribution as well.

Appendix: Theoretical Considerations on the Role of [^{13}C,^{13}C]-TROSY in TROSY-HCN Experiments

During the long $^{13}C\rightarrow{}^{15}N$ and $^{15}N\rightarrow{}^{13}C$ polarization transfer periods of the HCN experiment (Figure 2) the transverse relaxation of the $^{13}C1'$ and $^{13}C6$ coherences is determined largely by ^{13}C CSA interactions, $^{13}C-^{1}H$ DD couplings, $^{13}C-^{13}C$ DD coupling, and mutual interferences between these relaxation mechanisms. To gain insight into the relative importance of the different relaxation pathways we performed an analytical integration of the master equation for spin dynamics in a manner similar to that described by Salzmann et al.:[41]

$$f(T) \propto (\exp[-R_{CC}{}^{1'2'}T] + \exp[-R_{CC}{}^{3'4'}T])\exp[-(R_{CH}{}^{34} - 4J(0)\delta_C{}^2)T] \quad (3)$$

where $\mathbf{T} = 2\Delta + t_2$, $R_{CH}{}^{34}$ is the transverse relaxation rate of the transition 3→4 in the standard energy level diagram for the $^{13}C-^{1}H$ multiplet in the absence of $^{13}C-^{13}C$ interaction,[28] and $R_{CC}{}^{1'2'}$ and $R_{CC}{}^{3'4'}$ are the transverse relaxation rates of the transitions 1′→2′ and 3′→4′ in the $^{13}C-^{13}C$ multiplet in the absence of $^{13}C-^{1}H$ interaction. The relaxational interference between the $^{13}C-^{1}H$ and $^{13}C-^{13}C$ DD couplings is neglected, considering that this cross-correlation is suppressed because the angle between the two DD vectors is near 60°. For a rigid, isotropically tumbling spherical molecule in the slow motion limit, the rates $R_{CH}{}^{34}$, $R_{CC}{}^{1'2'}$, and $R_{CC}{}^{3'4'}$ are given by

$$R_{CH}{}^{34} = 4J(0)(p_{CH}{}^2 + \delta_C{}^2 - K_1 - K_2) \quad (4)$$

$$R_{CC}{}^{1'2'} = 4J(0)(p_{CC}{}^2 + \delta_C{}^2 + K'_1 + K'_2) \quad (5)$$

$$R_{CC}{}^{3'4'} = 4J(0)(p_{CC}{}^2 + \delta_C{}^2 - K'_1 - K'_2) \quad (6)$$

The coupling constants are defined as $p_{CH}{}^2 = (1/8)(\gamma_C\gamma_H\hbar/r_{CH}{}^3)^2$, $p_{CC}{}^2 = (5/32)(\gamma_C\gamma_C\hbar/r_{CC}{}^3)^2$, $\delta_C{}^2 = (1/18)(\omega_C\Delta\sigma_C)^2$, and $K_i = (1/6)\gamma_C\gamma_H\hbar\omega_C\Delta_i(3\cos^2\Phi_i - 1)/2r_{CH}{}^3$, where γ_C and γ_H are the gyromagnetic ratios of the C and H spins, $\hbar$ is the Planck constant divided by 2π, r_{CH} is the distance between the spins C and H, r_{CC} is the distance between two covalently linked carbon atoms, $(\Delta\sigma_C)^2 = \Delta_1{}^2 + \Delta_2{}^2 - \Delta_1\Delta_2$, with $\Delta_1 = \sigma_{33} - \sigma_{11}$ and $\Delta_2 = \sigma_{22} - \sigma_{11}$, and Φ_1 and Φ_2 are the angles between the C−H bond and the directions of σ_{33} and σ_{22} of the ^{13}C chemical shift tensor. Similarly, $K'_i = (1/6)\gamma_C\gamma_C\hbar\omega_C\Delta_i(3\cos^2\Phi'_i - 1)/2r_{CC}{}^3$, where the angles Φ'_1 and Φ'_2 are between the C−C bond and the principal directions of the chemical shift tensor. The following bond lengths were used: $r_{CH} = 0.1096$ nm for C1′−H1′, $r_{CH} = 0.1084$ nm for C6−H6, $r_{CC} = 0.153$ nm for C1′−C2′, and $r_{CC} = 0.136$ nm for C6−C5.[43]

Since we are not aware of the availability of experimental data for the ^{13}C CSA tensors of C6 and C1′ in nucleic acids, the directions and values of the principal components of the ^{13}C CSA tensors have been calculated by using density functional theory as implemented in the Gaussian 94 quantum chemistry program.[45] The MOLMOL program[46] was used to generate a molecular fragment consisting of a cytosine nucleoside containing a methyl group in the C5′ position. The geometry of the molecule was optimized using the B3LYP function with the 6-31G(d) basis set, which was followed by the CSA tensor calculations using the 6-311+G(3df,2p) basis set. For C6, the most highly shielded direction, σ_{33}, was thus found to be perpendicular to the plane of the aromatic ring, and the least shielded orientation, σ_{11}, is directed approximately along the $^{13}C-^{1}H$ bond, with average values of $\sigma_{11} = 209$ ppm, $\sigma_{22} = 112$ ppm, and $\sigma_{33} = 17$ ppm. Both σ_{33} and σ_{22} are thus orthogonal to the $^{13}C-^{1}H$ bond, resulting in $\Phi_1 = 90°$, $\Phi_2 = 90°$, $\Phi'_1 = 90°$, and $\Phi'_2 = 60°$. For C1′, $\sigma'_{11} = 197$ ppm, $\sigma'_{22} = 167$ ppm, and $\sigma'_{33} = 136$ ppm, with σ'_{11} approximately along the C1′−H1′ bond and σ'_{33} approximately perpendicular to the plane defined by H1′, C1′, and N1, which corresponds to $\Phi_1 = 90°$ and $\Phi_2 = 54°$, and $\Phi'_1 = 35°$ and $\Phi'_2 = 54°$. Using these parameters the relaxation rates of the base C6 carbon in the *Antp* homeodomain−DNA complex were estimated based on a correlation time of $\tau_c = 20$ ns:[27] $R_{CH}{}^{34} = 60\ s^{-1}$ (as compared to a relaxation rate from $^{13}C-^{1}H$ DD coupling and ^{13}C CSA of $169\ s^{-1}$ without the use of TROSY), $R_{CC}{}^{1'2'} = 60\ s^{-1}$, and $R_{CC}{}^{3'4'} = 31\ s^{-1}$ (as compared to a relaxation rate from $^{13}C-^{13}C$ DD coupling and ^{13}C CSA of $45\ s^{-1}$ without the use of TROSY). For the experimental setup of Figure 6, the calculated $R_{CC}{}^{1'2'}$ and $R_{CC}{}^{3'4'}$ relaxation rates predict a 1:2 ratio of the relative intensities of the two doublet components, which is in good agreement with the experiment.

Acknowledgment. Financial support was obtained from the Schweizerischer Nationalfonds (Project 31.49047.96), from the ETH Zürich for a special grant within the framework of the Swiss-Japanese R&D Roundtable Collaboration, and by CREST (Core Research for Evolutional Science and Technology) of the Japan Science and Technology Corporation (JST). We thank Dr. Akira Ono for the synthesis of the labeled DNA.

Supporting Information Available: Figure showing three pulse sequences (PDF). This material is available free of charge via the Internet at http://pubs.acs.org.

JA9938276

(44) Saenger, W. *Principles of Nucleic Acid Structure*; Springer: New York, 1992.

(45) Frisch, M. J.; Trucks, G. W.; Schlegel, H. B.; Gill, P. M. W.; Johnson, B. G.; Robb, M. A.; Cheeseman, J. R.; Keith, T.; Petersson, G. A.; Montgomery, J. A.; Raghavachari, K.; Al-Laham, M. A.; Zakrzewski, V. G.; Ortiz, J. V.; Foresman, J. B.; Cioslowski, J.; Stefanov, B. B.; Nanayakkara, A.; Challacombe, M.; Peng, C. Y.; Ayala, P. Y.; Chen, W.; Wong, M. W.; Andres, J. L.; Replogle, E. S.; Gomperts, R.; Martin, R. L.; Fox, D. J.; Binkley, J. S.; Defrees, D. J.; Baker, J.; Stewart, J. P.; Head-Gordon, M.; Gonzalez, C.; Pople, J. A. *Gaussian94*; Gaussian Inc.: Pittsburgh, PA, 1995.

(46) Koradi, R; Billeter, M.; Wüthrich, K. *J. Mol. Graph.* **1996**, *14*, 51−55.

(47) Shaka, A. J.; Barker, P.; Freeman, R. *J. Magn. Reson.* **1985**, *64*, 547−552.

(48) Messerle, B. A.; Wider, G.; Otting, G.; Weber, C.; Wüthrich, K. *J. Magn. Reson.* **1989**, *85*, 608−613.

(49) Marion, D.; Ikura, M.; Tschudin, R.; Bax, A. *J. Magn. Reson.* **1989**, *85*, 393−399.

(50) Kay, L. E.; Keifer, P.; Saarinen, T. *J. Am. Chem. Soc.* **1992**, *114*, 10663−10665.